water

MDPI

Article

Sand/Polyethyleneimine Composites with Enhanced Sorption/Desorption Properties toward Pollutants

Florin Bucatariu [1], Larisa-Maria Petrila [1], Marius-Mihai Zaharia [1], Frank Simon [2] and Marcela Mihai [1,*]

[1] Petru Poni Institute of Macromolecular Chemistry, 41A Grigore Ghica Voda Alley, 700487 Iasi, Romania
[2] Leibniz-Institut für Polymerforschung Dresden e.V., 6 Hohe Str, 01069 Dresden, Germany
* Correspondence: marcela.mihai@icmpp.ro; Tel.: +40-332-880-220

Abstract: The direct deposition of polyethyleneimine (PEI), a weak polycation with a large content of amino groups, onto sand fractions with different sizes (F70, F100, F200, and F355), resulted in versatile core-shell sorbents for water cleaning. Herein, PEI and the weak polyanion poly(acrylic acid) (PAA) were directly precipitated as an nonstoichiometric polyelectrolyte complex ([PEI]:[PAA] = 2:1) onto a sand surface followed by cross-linking with glutaraldehyde (GA) at three molar ratios ([CHO]:[amine] = 1:10; 1:5; 1:1 = r). Non-crosslinked polyelectrolyte chains were washed out in strongly basic (pH 14) and acidic (pH 0) media. The sand/PEI-GA composites were evaluated to determine the organic shell stability using swelling experiments and X-ray photoelectron spectroscopy. The sorbed/desorbed amount of two model pollutants (copper ions and bromocresol green) in column experiments depended on the sand fraction size and cross-linking degree of the PEI shell. The maximum recorded values, after five loading/release cycles of pollutant species onto F70/PEI-GA_r, F100/PEI-GA_r, F200/PEI-GA_r, and F355/PEI-GA_r, were situated between the 0.7–5.5 mg Cu^{2+}/mL column and 3.7–15 mg BCG/mL column. Sand/PEI-GA_r composites could act as promising sorbents, low-cost and eco-friendly, which could be applied for water purification procedures.

Keywords: composite sorbent; column experiment; water cleaning; bromocresol green; copper ions

check for updates

Citation: Bucatariu, F.; Petrila, L.-M.; Zaharia, M.-M.; Simon, F.; Mihai, M. Sand/Polyethyleneimine Composites with Enhanced Sorption/Desorption Properties toward Pollutants. *Water* **2022**, *14*, 3928. https://doi.org/10.3390/w14233928

Academic Editor: Alexandre T. Paulino

Received: 26 October 2022
Accepted: 29 November 2022
Published: 2 December 2022

Publisher's Note: MDPI stays neutral with regard to jurisdictional claims in published maps and institutional affiliations.

Copyright: © 2022 by the authors. Licensee MDPI, Basel, Switzerland. This article is an open access article distributed under the terms and conditions of the Creative Commons Attribution (CC BY) license (https://creativecommons.org/licenses/by/4.0/).

1. Introduction

Water is one of the most important natural resources on Earth, with a crucial role in the quality of life for humans, as well as for plants and animals. The global water demand is continuously increasing due to the expansion in the human population, but also because of the growing industrial requirements. Unfortunately, the increasing water demand is also connected with the increase in water pollution, with recent studies drawing attention to the health-related risks of water contamination [1–4]. Pollutants resulting from industrial processes as well as from agriculture, animal husbandry, and household use get into water bodies, are dissolved there, pass through the sewage treatment plants more or less unchanged, and possibly end up back in the drinking water sources. Among the most well-known contaminants in water, metal ions, dyes, pharmaceutical compounds, polycyclic aromatic hydrocarbons, cleaning products, and pesticides are of rising significance because of their potential cytotoxicity, endocrine disruption, and carcinogenic effects [5,6].

Different water treatment methods have been developed over the years, including filtration, sorption, membrane technology, coagulation, sedimentation, etc. [7–10]. Nevertheless, these methods are almost ineffective for the removal of complex contaminant mixtures that are found in waters. Based on this shortage, the research community has focused its attention on the development of new wastewater treatment methods, able to retain different types of pollutants and improve the overall quality of water supplies [11–14]. Among the methods developed for water treatments, of special interest is the use of nanotechnology and polymer science in the establishment of effective treatment techniques. The use of nanotechnology for water treatment is focused on different methods such as the fabrication

of nanosorbents and composite nanomembranes, the detection of contaminants in water, and the enhancement of pollutants degradation in photocatalytic processes [15–18]. Nevertheless, the use of nanotechnology is costly and difficult to use on large-scale processes, being mostly limited to the laboratory scale.

Natural and synthetic polymers are also of interest for water cleaning purposes. They can be used as flocculants, coatings for membranes, and also for the low-cost fabrication of different types of sorbents for pollutants such as fibers [19], resins [20], or core-shell particles [21]. The main advantage of polymer-based composite materials is that they can be successfully employed as sorbents for a variety of pollutants as demonstrated by the extensive research in this field [22–27]. The vast majority of natural polymers used in water treatment are polyelectrolytes, which are characterized by the existence of charged functional groups that can interact with oppositely charged contaminants [28]. Moreover, natural polymers are characterized by their high disponibility and biodegradability which reduces the environmental impact of their use in industrial processes. Among the synthetic polymers used, poly(ethyleneimine) (PEI), poly(acrylic acid) (PAA), poly(allylamine hydrochloride), and poly(methacrylic acid) are of high interest due to their availability and their ionic character that favors the retention of oppositely charged pollutants [29–31]. Charged polymers can be assembled in different structures to maximize the number of functional groups available to retain the target pollutants and exhibit impressive sorption capacity for different types of contaminants. Extensive research on the layer-by-layer assembly of polyelectrolytes and the subsequent use of the core-shell composites obtained for water treatment has already been completed [32–34], demonstrating that polymer-based composite materials can be successfully employed in the retention of dyes, pharmaceutical compounds, or metal ions from wastewater, even in competitive conditions.

Recently, a novel fabrication method for polymer-based sand composite materials was reported, by covering sand microparticles with a coacervate of polyelectrolyte complexes, then polycation chemical cross-linked and polyanion extraction out of the reticulate polycation framework, composites that can potentially be used for water treatment [35]. The proposed fabrication method reduces the economic and environmental impact of sorbent fabrication, preserving the availability of a high number of functional groups. In this subsequent study, the influence of the sand core size (70 to 355 μm) and shell cross-linking degree (r = [CHO]:[amine] = 1:10; 1:5; 1:1) on the core-shell stability during synthesis as well as the dynamic sorption behavior towards two model pollutants, a small metal ion (Cu^{2+}) and a large dye molecule, bromocresol green (BCG) were examined in depth.

2. Materials and Methods

2.1. Materials

The sand microparticles (collected from Rasca river basin) were treated with NaOH and HCl to remove humic acids and carbonates, washed, dried, and sieved by a Retsch vibratory sieve shaker (Retsch LLC, Haan, Germany) using six different mesh sized sieves (70, 100, 180, 200, 355, and 425 μm), at 90 Hz frequency. The obtained sand fractions were collected after 15 min, (F < 70, F70, F100, F180, F200, F355 and F > 425, where the numbers represent the mesh size of each sieve). The weak polyelectrolytes, branched poly(ethyleneimine) (PEI) (M_w = 25,000 g·mol^{-1}), and PAA (M_w = 10,000 g·mol^{-1}) were provided by Aldrich. The inorganic salt of $CuSO_4 \cdot 5H_2O$ (Sigma-Aldrich) and bromocresol green (Alfa Aesar) were used as received. Ethylenediaminetetraacetic acid as aqueous sodium salt ($EDTANa_2$) was acquired from Aldrich. Sodium hydroxide p.a. pellets from Riedl-de Haën were used without further purification. Hydrochloric acid, 36% solution, from Chemical Company was used as received.

2.2. Synthesis of Sand Composites

For increasing the amount of functional groups on the sand surface, branched PEI and PAA with a high number of amino groups and carboxylic groups were used, respectively. The high concentration of PEI and PAA solutions, and polymers with low molecular masses,

a non-stoichiometric interpolyelectrolyte complex (PEI_2/PAA_1) was successfully deposited on the sand microparticles surface (Scheme 1) by an in situ precipitation method under vigorous mechanical mixing [35], generating a sticky assembling of all microparticles in one big aggregate. The main driving forces of complex deposition were the electrostatic interactions between anionic/cationic functional groups, hydrogen bonds, and hydrophobic interactions between the in situ formed complex and the solid sand surface.

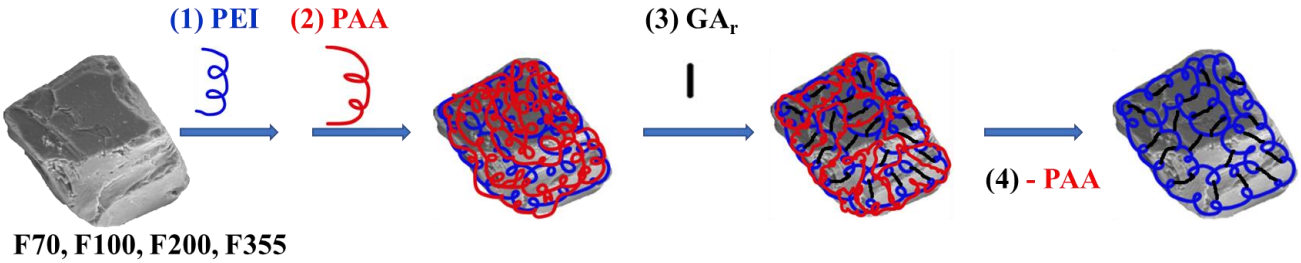

Scheme 1. Schematical representation of sand/PEI-GA_r composites by the complex precipitation on sand microparticles and PEI cross-linking with GA (r = [CHO]:[amine] = 1:10, 1:5 and 1:1) and PAA extraction from composite shell.

Using 10 mL of each sand fraction (F70, F100, F200, F355) mixed with 4.5 mL PEI solution (1 M) and 2.25 mL PAA solution (1 M, added drop-by-drop in the system), the following composites were obtained $F_n/(PEI_2/PAA_1)$, n = 70, 100, 200, and 355. At the end of the deposition process, the (PEI_2/PAA_1) organic shell successfully adhered to the sand surface based on the stickiness property of the polyelectrolyte complex, mainly due to the PAA chains. Thus, each sand fraction was functionalized with the same amount of complex but differently distributed on the external surface of the particles, which is a function of the fraction's average diameter. The amount of sand fraction and polyelectrolyte concentrations were kept constant in all depositions (steps 1 and 2 in Scheme 1), and only the particle sand diameters were different.

To stabilize the organic film around each particle, the sand/(PEI_2/PAA_1) composites were cross-linked with GA (OHC-CH_2-CH_2-CH_2-CHO) at three molar ratios (r = [CHO]:[amine] = 1:10, 1:5, and 1:1) for three hours. The GA molecule is a bifunctional reagent with a high reactivity towards the primary and secondary amino groups of PEI. This reaction was necessary to ensure the composite shell's stability in subsequent applications, where the high concentration and accessibility of the functional groups situated on the sand composite surface are very important. To ensure the flexibility of PEI chains around composite microparticles, the PAA and non-cross-linked PEI chains were extracted in strong basic and acidic media (1 M NaOH, and 1 M HCl), respectively. Thus, the following composites with sand were prepared: F70/PEI-GA_r, F100/PEI-GA_r, F200/PEI-GA_r, and F355/PEI-GA_r, where r is the cross-linking degree.

2.3. Sand Composite Indirect/Direct Characterization Methods

UV-Vis measurements (UV-VIS SPEKOL 1300 spectrophotometer, Analytik Jena, Germany) were performed to determine the concentration of Cu^{2+}, as PEI_4-Cu^{2+} complex (λ = 275 nm or λ = 622 nm), and BCG (λ = 616 nm) in aqueous solution, before and after sorption/desorption in/from the column. The chelation process between PEI and Cu^{2+} changed the absorption spectrum of aqueous solution, two broad bands appeared at 220–410 nm and 510–720 nm [36]. In these regions no bands appeared for individual components (PEI or Cu^{2+}). From the reported results, the detection was reliable due to the high stability of PEI-Cu complex at room temperature. The detection limit for copper ions was situated around 3 μM. The maximum stoichiometry or molar ratio between copper ions and amino groups of PEI is 1:4. To calculate the exact concentration of PEI solution used for copper detection a poly(sodium ethylenesulfonate) standard solution (10 mM) from BTG Company was used. Calibration curves (y_{Cu2+} = 0.067x or y_{Cu2+} = 0.0026x, and

y_{BCG} = 0.062x) were constructed and further used in the concentration determination of Cu^{2+} and BCG solutions. The Cu^{2+} and BCG amounts in each collected effluent fraction (q_e = mg/mL column) were determined using Equation (1):

$$q_e = (C_i - C_e)\cdot(V_{ef} \cdot m), \quad (1)$$

where C_i and C_e are the influent and effluent concentrations (mg/L), V_{ef} is the volume of effluent fraction, and m is the mass or volume of composite inside the column.

The swelling degree of the composites and the stability of the core/shell composites were estimated by measuring the volume of sediments in 15 mL plastic flasks during the entire swelling process (hydration, base, and acid extraction of non-crosslinked polyelectrolyte chains).

The size and shape of each sand fraction were evaluated using a particle characterization system (Morphologi G3SE, Malvern, UK). The microparticles were spread on the surface using the integrated dry powder disperser for enhanced separation of individual particles enabling the optimization of the measurement process.

FT-IR spectra of sand and its composites were acquired with the IRTracer-100 spectrometer (Shimadzu, Tokyo Japan), with ATR module (Pike Technologies, Madison, WI, USA), using 45 scans with a resolution of 4 cm^{-1}.

X-ray diffraction (XRD) was performed on F100 sand fraction before and after polymer deposition, in the angular range (2θ) of 15° to 90°, at a scanning step of 0.01° and a recording rate of 2°/min, using a Rigaku Miniflex 600 diffractometer (Rigaku, Tokyo, Japan). Background subtraction, smoothing and WPPF (Whole Powder Pattern Fitting) refinement of XRD data were made using the SmartLab II v.4 software (Rigaku, Tokyo, Japan) package for powder X-ray diffraction analysis, while the diffraction peaks were identified using the Crystallography Open Database (COD).

X-ray photoelectron spectroscopy (XPS) measurements were performed with an Axis Ultra X-ray photoelectron spectrometer (Kratos Analytical, Manchester, UK). The method offers qualitative and quantitative information on the elements on the sand sample (initial and as composite, as well as after extraction process). The spectrometer was equipped with a monochromatic Al Kα (h·ν = 1486.6 eV) X-ray source of 300 W at 15 kV. Using a hemispheric analyzer, the kinetic energy of photoelectrons was determined with a pass energy of 160 eV and 20 eV for wide-scan and high-resolution spectra, respectively. A low-energy electron source working in combination with a magnetic immersion lens were applied to avoid the electrostatic charging of the sample. Later, the recorded peaks were shifted to set the C 1s peak to 285.00 eV. Normalized peak areas were calculated from the recorded peak areas considering experimentally determined element-specific sensitivity factors and the spectrometer transmission function.

2.4. Dynamic Loading and Release of Cu^{2+} and BCG onto/from Sand Composites

The Cu^{2+} and BCG dynamic sorption properties of the F70/PEI-GA_r, F100/PEI-GA_r, F200/PEI-GA_r and F355/PEI-GA_r samples were investigated in dynamic conditions, using a fixed-bed OMNIFIT glass column (total length of 8 cm with 6.6 mm inner diameter, volume (mL) = 0.3421 × bed height (cm)). For all tests, a constant flow rate of 2 mL/min was set-up by a Shenchen peristaltic pump (Shenchen Precision Pump Co., Baoding, China). The 100 mg or 2 mg Cu^{2+}/L and 350 mg BCG /L influent concentration as well as the volume of each composite (1.37 mL) inside the column were kept constant during all dynamic experiments. The pH of each influent solution (copper or BCG) varied between 4.5 and 5.2. The exhausted columns were regenerated, either with 0.01 M $EDTANa_2$ for the extraction of Cu^{2+} or with 1 M NaOH to remove BCG from the composites, then rinsed with distilled water. The NaOH solution enabled the fast desorption of BCG from core/shell composite surface, as a result of the deprotonation of the carboxylic groups. The break-through time (t_b, min) (the time at which concentration of pollutant reaches 5% from initial concentration) [37] and the exhaustion time (t_e, min) (the time at which

concentration of pollutant reaches 95% from initial concentration) were determined using the breakthrough curves. The Thomas and Yoon–Nelson models were applied to calculate the dynamic sorption parameters.

3. Results

Sand represents a cheap and accessible material with strong mechanical properties which can be used as a core in the synthesis of core/shell composite microparticles, with potential application in water treatment. In this study, core/shell sand/polyelectrolytes microparticles were obtained by keeping constant the deposited amount of polyelectrolytes and varying the sand fraction size and the cross-linking degree, the adaptability and the organic shell steadiness on sand surface were studied as well as the dynamic sorption properties of two model pollutants, a heavy metal ion (Cu^{2+}) and an anionic dye molecule (BCG).

3.1. Sand Characterization

The polydisperse sand sample griddling resulted in six fractions collected on the sieves (F > 425, F355, F200, F100, F70, and F < 70), where the numbers represent the mesh size of each sieve. Before sieving, the sand microparticles were treated with NaOH and HCl to remove humic acids and carbonates. Discarding the extreme sized fractions (F > 425 and F < 70), a number of four fractions, which represented approximately 80% of the initial sand sample, were subsequently used to obtain the core/shell composites. The mass distribution of sand microparticles, as well as the size polydispersity, shown in Figure 1, was obtained by weighting the samples and by Morphologi G3SE analysis.

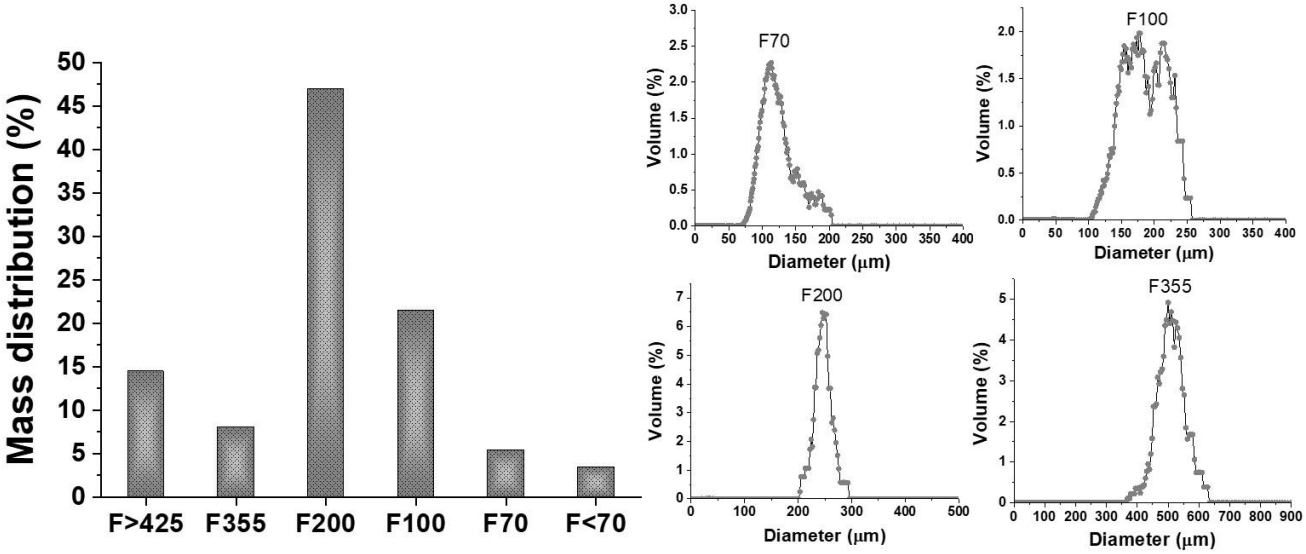

Figure 1. Mass distribution and size polydispersity of each sand fraction.

For the coacervate precipitation experiments onto the sand fractions, just the outside area of microparticles should be considered since the inner part of the sand microparticle is not accessible to the interpolyelectrolyte complex chains. The external surface of a sand fraction could be roughly approximated with the formula: $S = 4\pi \cdot (\text{diameter}/2)^2$. Due to the presence of aluminum-silicates in the sand structure, the negatively charged surface of the sand was due to the dissociation of the Al-OH and Si-OH surface groups in aqueous media. Thus, the negatively charged sand surface could interact more strongly with polycations more than polyanions in an acidic, neutral, or basic environment.

3.2. Sand/PEI Composites

The degree of PEI cross-linking inside the shell is a significant parameter in the sorption/desorption of different types of pollutant molecules on the composite surfaces. Strong

composite cross-linking (r = 1:1) will result in a PEI-GA_r shell with a strong packing of the polymeric chains, with less accessibility for the pollutant molecules to the active sorption site, but with a higher density of the functional groups. Instead, low composite cross-linking degrees (r = 1:10) will create more flexible shells with fast accessibility towards active functional groups, but with lower stability of the organic architecture under environmental conditions. In this study, the amount of the composite shell which remained and surrounded each sand particle after deposition/cross-linking/extraction processes, was evaluated in swelling experiments by measuring the volume of sediments for each sand fraction (Figure 2).

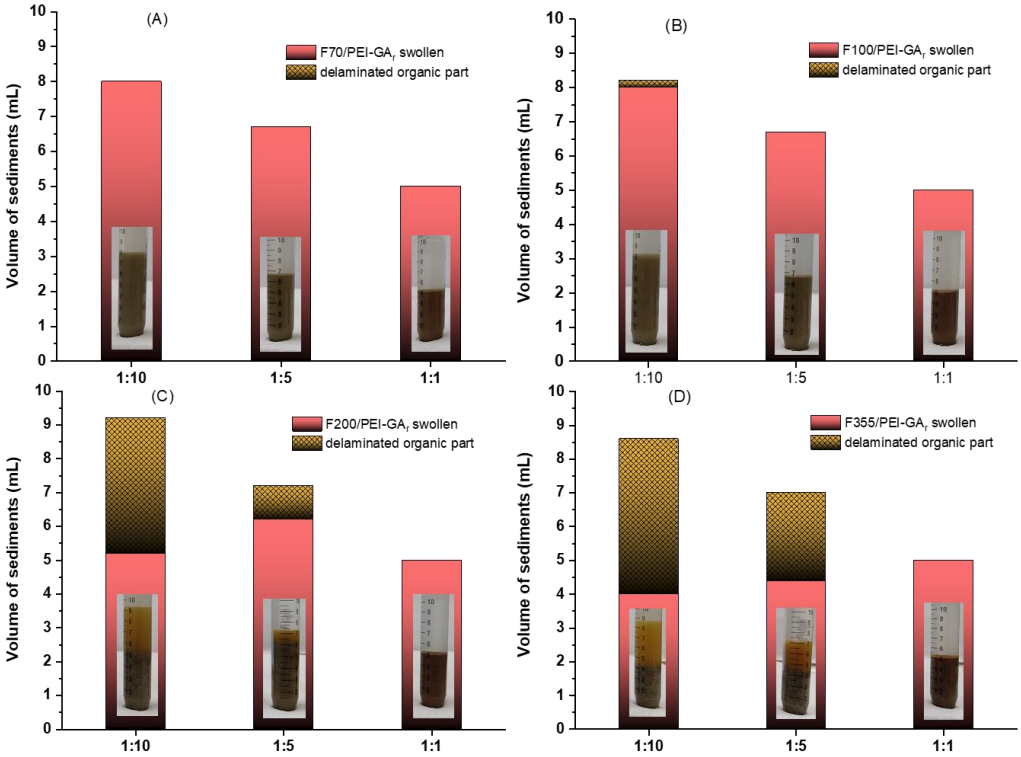

Figure 2. Volume of composite sediments for each functionalized sand fraction ((**A**) = F70, (**B**) = F100, (**C**) = F200 and (**D**) = F355) as a function of the cross-linking degree (r = 1:10, 1:5 and 1:1) measured after strong base and acid treatment.

It was observed that the PEI-$GA_{1:1}$ shell, with the strongest cross-linking density, was the most stable between all the composites in the acid–base treatments performed. In this case, r = 1:1, the swelling degree was minimal, and no delamination of organic composite parts was observed. The PEI-$GA_{1:10}$ shell, with the lowest cross-linking density, was less stable in acid and base media in the case of composites with a higher core size (Figure 2C,D). The composite with the smallest core size (F70/PEI-$GA_{1:10}$) presented the highest degree of swelling (highest volume of sediments) without any delamination of the shell. The fraction F70, with the smallest core size, presented the highest surface area as compared to other fractions (F100, F200, and F355). The PEI deposited amount was kept constant for each sand fractions; this meant that this fraction would contain the thinner organic layer on the solid surface. In the cross-linking step the GA molecules will diffuse easier in the thinner layers, F70 case, compared with higher core size fractions with thicker layers, and therefore the cross-linking yield for the smaller composite will be the highest. Thus, the resulted F70 sand composites will contain the most stable cross-linked shell due to the easiest accessibility of GA to the amino groups of deposited PEI. Based on these observations, it was concluded that the loss of the organic shell increased with the sand size, for the same cross-linking degree, and decreased with the cross-linking degree, for the same sand fraction. Using the volume of sediments as a characterization method during the acid–base treatment of each

type of composite, it was possible to estimate the stability of each shell as a function of the core size and cross-linking degree.

The direct deposition of organic polyelectrolyte chains onto the sand surface was demonstrated by FTIR spectroscopy, comparing the fingerprint zone of F100 and F100/PEI-$GA_{1:10}$ spectra (Figure 3).

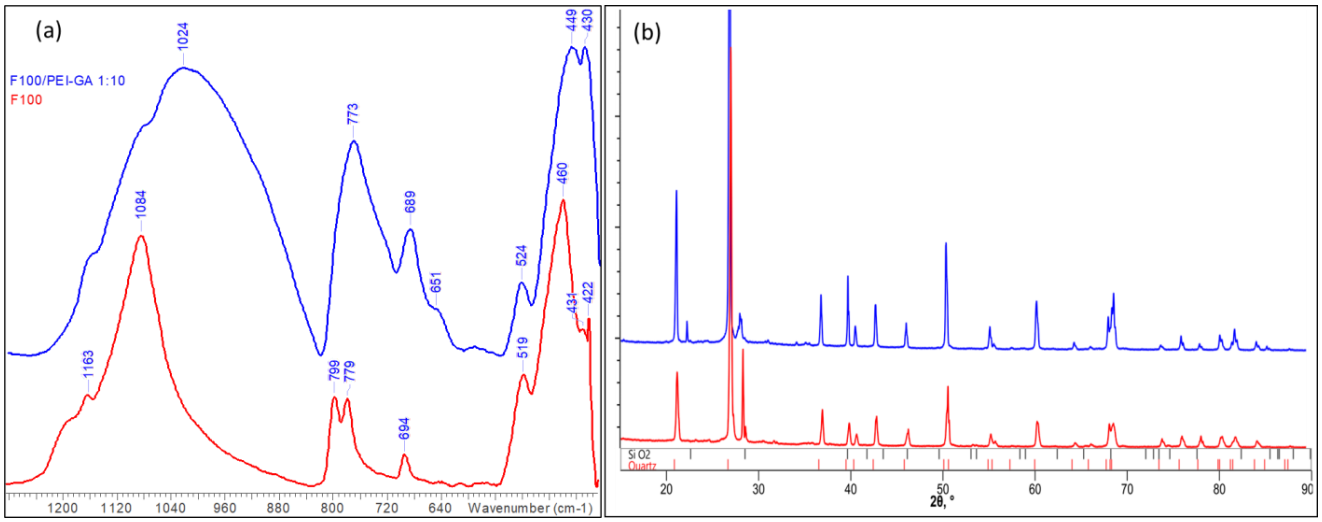

Figure 3. (**a**) FTIR spectra of and (**b**) XRD diffractograms of F100 (red) and F100/PEI-$GA_{1:10}$ (blue) microparticles.

The FT IR spectrum of the F100 sample (Figure 3a) showed a doublet of weak and strong bands at 1163 and 1084 cm^{-1}, assigned to Si-O-Si and SiO stretching vibrations, as well as for low Si for Al or Fe^{3+} substitution, suggesting the presence of quartz. The stretching vibration observed as doublet at 799 and 779 cm^{-1} and the symmetrical bending vibration of the Si-O group at 694 cm^{-1} indicates that the silica was in the form of α-quartz [38]. The bands observed at 513 and 460 cm^{-1} were attributed to O-Si-O, Si-O-Al, and Si-O-Si bending modes. The FTIR spectrum of F100/PEI-$GA_{1:10}$ microparticles kept the main characteristics of the bare sand in the 400-530 cm^{-1} domain. Nevertheless, the band broadening in the region 1200–850 cm^{-1}, with the highest peak at 1024 cm^{-1}, was ascribed both to the sand substrate and to functional groups in PEI and GA, such as CH_2 (wag, 1165 cm^{-1}), C-O (stretch, 1024 cm^{-1}), C-N (stretch, 1151 cm^{-1}), and C-H (bend, 1019 cm^{-1}). Moreover, the doublet at around 780 cm^{-1} was not visible, being most probably included in the larger peak with the highest intensity at 773 cm^{-1}, with the contribution of C-H deformation vibration of macromolecular backbone. The peak of Si-O group at 694 cm^{-1} was shifted to 689 cm^{-1} along with the appearance of that at 651 cm^{-1} due to N-H bond vibration. These observations were also supported by X ray diffraction (Figure 3b), with both SiO_2 and quartz being found in the sand sample (Table 1). Moreover, both XRD diffractograms shared the same values of 2θ, the SiO_2 and quartz lattice parameters were almost unchanged after the deposition of polyelectrolytes, meaning that the inorganic core was not affected during the organic shell deposition.

Table 1. F100/PEI-$GA_{1:10}$ samples.

Sample	Phase Name	Wf, wt%	Lattice Parameters, Å			V_L, Å	S	COD Card No.
			a	b	c			
F100	SiO_2	56.1	4.565	4.565	5.411	95.113	1.041	1,536,409
	Quartz	43.9	4.919	4.919	5.407	112.422		9,012,600
F100/PEI-GA1:10	SiO_2	69.3	4.445	4.445	5.062	86.605	1.062	1,536,409
	Quartz	30.7	4.849	4.849	5.401	109.388		9,012,600

Note: Wf—polymorph weight fraction, VL—lattice volume, S—"goodness-of-fit".

Further, to analyze the effect of the core size and PEI cross-linking degree on the organic shell, all functionalized core-shell sand fractions (F70/PEI-GA_r, F100/PEI-GA_r, F200/PEI-GA_r) were characterized by XPS, as a qualitative and quantitative method of surface investigation (Figure 4). The organic shell of cross-linked PEI-GA_r brings significant quantities of nitrogen and carbon atoms on the sand surface. The XPS survey spectra recorded from the sand fraction F100 showed the presence of the following elements: iron (Fe 2s, Fe 2p, Fe 3p peaks and Fe LMM Auger series), aluminum (Al 2p and Al 2s peaks), calcium (Ca 2p peaks), magnesium (Mg KLL Auger series), oxygen (O 1s, O 2s peaks and O KLL Auger series), carbon (C 1s) and silicon (Si 2s and Si 2p peaks) (Figure 4a). The presence of these peaks in the XPS spectra demonstrated that the natural sand sample was an aluminum silicate which carried organic impurities on the grain surfaces (carbonates have been removed during the acidic treatment of the sand with HCl 1 M).

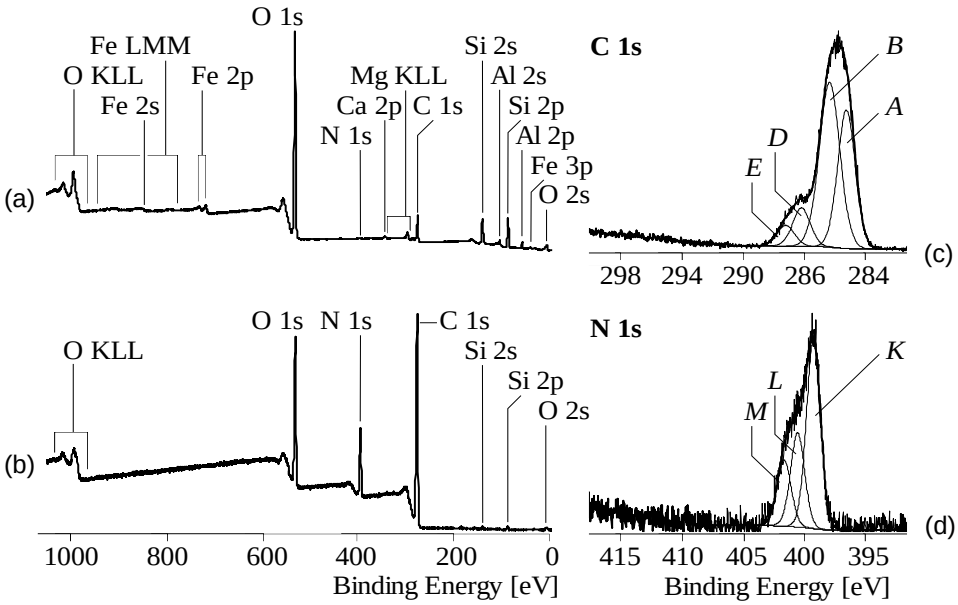

Figure 4. XPS survey spectra of unmodified F100 sand fraction (**a**) and F100/(PEI_2/PAA_1)-$GA_{1:10}$ composite (**b**) and XPS high resolution spectra of C 1s (**c**) and N 1s (**d**) obtained for the same composite surface.

After deposition of the interpolyelectrolyte PEI_2/PAA_1 coacervate onto sand fractions and the subsequent cross-linking of the shell with GA (r = 1:10), the modified sand fractions F100/(PEI_2/PAA_1)-$GA_{1:10}$ exhibited intense N 1s and C 1s peaks due to the presence of the polyelectrolyte backbones carrying functional groups (Figure 4b). The high-resolution C 1s spectrum shown as an example for the sand composite materials (Figure 4c) was deconvoluted into four component peaks. Component peak A arising at 285.00 eV resulted from hydrocarbons (ACxHy) which do not have heteroatoms in their immediate neighborhood. Photoelectrons escaped from carbon atoms, which were bonded to nitrogen were collected as component peak B at 286.04 eV. Thus, this component peak can be considered as

evidence for the presence of the PEI's amino groups. However, azomethine groups, which were formed by cross-linking reactions of the amino groups with glutaraldehyde were presented by component peak B (BC=NR). PAA molecules can be identified by component E at 288.75 eV. This component peak was caused by photoelectrons from the carbonyl carbon atoms of the carboxylic acid groups (HO-EC=O). Interactions of the PAA's carboxylic acid groups and the PEI's amino groups led to salt-like ion pairs (-$COO^{\ominus}\cdots H^{\oplus}\cdots$NRH-) via the deprotonation of the carboxylic acid groups and the protonation of the amino groups, which can be considered as a precursor to carboxylic amide formation. Carbonyl carbon atoms involved in such salt-like bonds ($^{\ominus}$O-^{D}C=O ↔ O=^{D}C-$O^{\ominus}$) were observed as component peak D at 287.77 eV. Photoelectrons from carbon atoms in the α-position to the carbonyl carbon atoms of the carboxylic acid groups (-^{B}C-^{E}COOH) contributed to component peak B. Thus, the intensity of component peak B was approximately twice the [N]:[C] ratio determined from the survey spectrum ([N]:[C] = 0.22) plus the intensity of component peak E. The wide N 1s spectrum (Figure 4d) was decomposed into three component peaks. The component peak K with the lowest binding energy value (399.28 eV) shows the amino groups of the PEI molecules (-^{B}C-^{K}NR). Azomethine groups (^{B}C=^{L}NR) were detected as component peak L at 400.56 eV. Nitrogen species protonated by the PAA's carboxylic acids or acidic wash (-^{B}C-$^{M}N^{\oplus}$HR) were observed as peak M at 401.66 eV.

Quantitative information could be obtained from the normalized intensities of the N 1s, C 1s and the Si 2p peaks (converted into atomic concentrations), which could represent a measure of the deposited amount of polyelectrolytes onto each composite with different core sizes and cross-linking degrees (r = 1:10, 1:5, and 1:1) (Table 2). From the determined atomic concentrations, an approximate complete coverage of the sand core with the polyelectrolyte shell was observed, the silicon atoms concentration being less than 1%. The increase in the C 1s atomic concentration values with the increase in the cross-linking degree, for the same core size demonstrated that a higher organic amount was present in the composite at a higher cross-linking degree. Moreover, the decrease in nitrogen concentration with the increase in the cross-linking degree demonstrated, also, the success of GA cross-linking reactions. After the cross-linking, more carbon atoms remained on the composite surface due to the stabilization of the shell around each sand particle.

Table 2. Atomic concentrations of carbon, nitrogen, and silicon on the surface of the composites.

Composite		Atomic Concentration (%)		
Core	**Shell**	**C 1s**	**N 1s**	**Si 2p**
F70	PEI-$GA_{1:10}$/PAA	69.69	14.81	0.67
	PEI-$GA_{1:5}$/PAA	74.23	14.07	0.71
	PEI-$GA_{1:1}$/PAA	74.82	10.41	0.37
F100	PEI-$GA_{1:10}$/PAA	69.33	13.30	0.63
	PEI-$GA_{1:5}$/PAA	71.53	13.13	0.74
	PEI-$GA_{1:1}$/PAA	73.45	9.81	0.82
F200	PEI-$GA_{1:10}$/PAA	72.93	14.35	0.88
	PEI-$GA_{1:5}$/PAA	70.43	13.20	0.65
	PEI-$GA_{1:1}$/PAA	75.62	11.31	0.40

After the deposition of the polyelectrolytes and GA cross-linking of the composite shell, the free PAA chains were removed in strongly basic media. Moreover, to remove the PEI chains which were not involved in the shell network, the composites were treated with HCl 1 M aqueous solution. Using these two aggressive pH treatments, some of the polyelectrolyte chains were removed from the cross-linked shell. This fact was demonstrated by the decrease in the atomic ratios of elements ([C 1s]/[Si 2p] and [N 1s]/[Si 2p] after acid–base treatment for chain extraction (Figure 5).

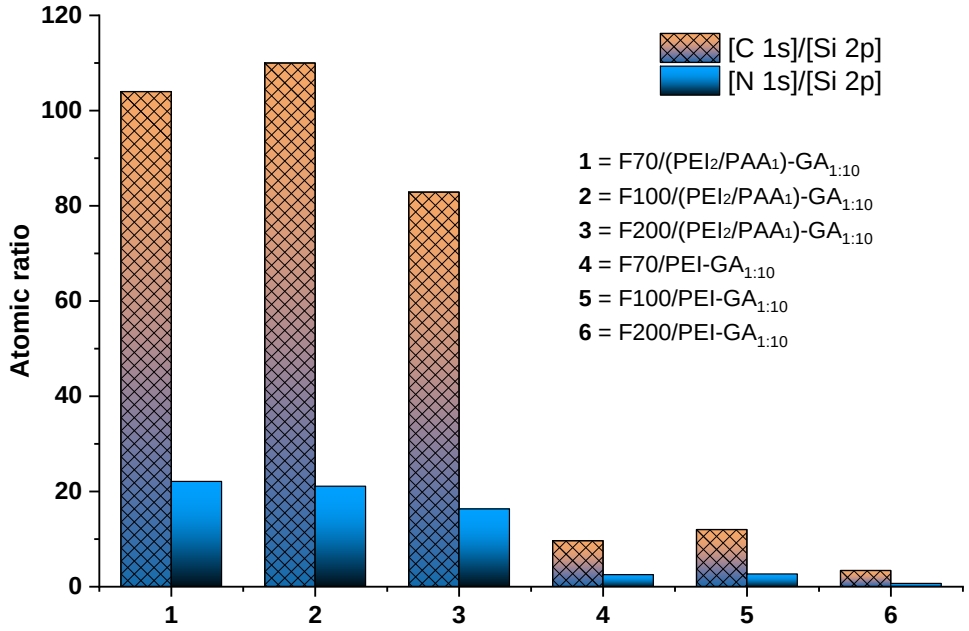

Figure 5. Atomic ratios calculated from XPS survey spectra for composite sand fractions, before (1, 2, 3) and after (4, 5, 6) the extraction of non-crosslinked polyelectrolyte chains in acid-base media.

As shown in Figure 5, the atomic ratios decreased drastically after the acid-base extraction, compared with the values recorded before extraction. The decreases of non-cross-linked PEI and PAA content by multiple extraction/washing were smaller for composites with smaller cores (F70 and F100) than for the composites with the biggest core (F200), where the loss of non-cross-linked PEI and PAA chains was higher in the successive extraction/washing steps. Thus, the XPS measurements showed that the PEI-GA_r composites contained smaller amounts of organic shells compared with the (PEI_2/PAA_1)-GA_r ones, but with a more flexible PEI network around the sand particles and a higher number of functional groups that were more accessible to the pollutant molecules, such as copper ions and BCG molecules.

3.3. Dynamic Copper Ions and Dye Molecules Sorption onto Sand/PEI-GA_r Composite Microparticles

To test the versatility and accessibility of the composite functional groups towards small ions, such as Cu^{2+}, or large molecules, such as the anionic dye BCG, experiments in dynamic conditions in continuous or discontinuous modes were carried out. In the first column set-up experiment, the maximum sorption capacity of all composites towards Cu^{2+} ions dissolved in aqueous solution (C_i = 100 mg/L mM) was determined (Figure 6).

The maximum sorbed amount of Cu^{2+} was achieved for the F70/PEI-$GA_{1:10}$ and F100/PEI-$GA_{1:10}$, the composites with the highest swelling degree and with the smallest core size. These core/shell composites with a low degree of cross-linking and a low core size presented a high surface area with more functional groups involved in copper retention. The sorption capacity towards Cu^{2+} of the composites with small cores (F70 and F100) decreased with the increase in the cross-linking degree due to the slow diffusion of the ions through the dense polyelectrolyte chains. In the case of the composites with a higher core size (F200 and F355), the retention capacity increased with the cross-linking degree due to the higher amount of shell present on the sand surface at a higher cross-linking degree. As shown above, in the stability tests and XPS measurements, the composites with large cores lost more organic material at low cross-linking degrees as compared to other composites.

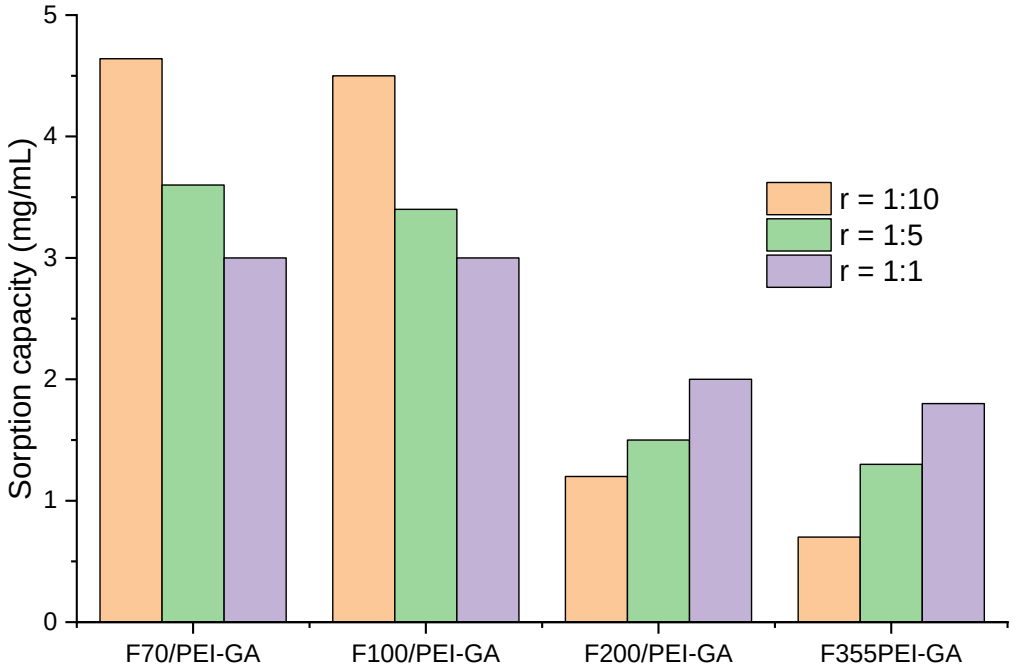

Figure 6. Maximum sorption capacity of the composite sand fractions evaluated in dynamic conditions in column (C_{Cu}^{2+} = 100 mg/L, Flow = 2 mL/min) (continuous mode).

The column experiments on Cu^{2+} removal from aqueous solution (C_i = 100 mg/L) are presented in Figure 7. Using a peristaltic pump, the aqueous solution was introduced with a flow of 2.0 mL/min in a column filled with 1.4 mL sorbent.

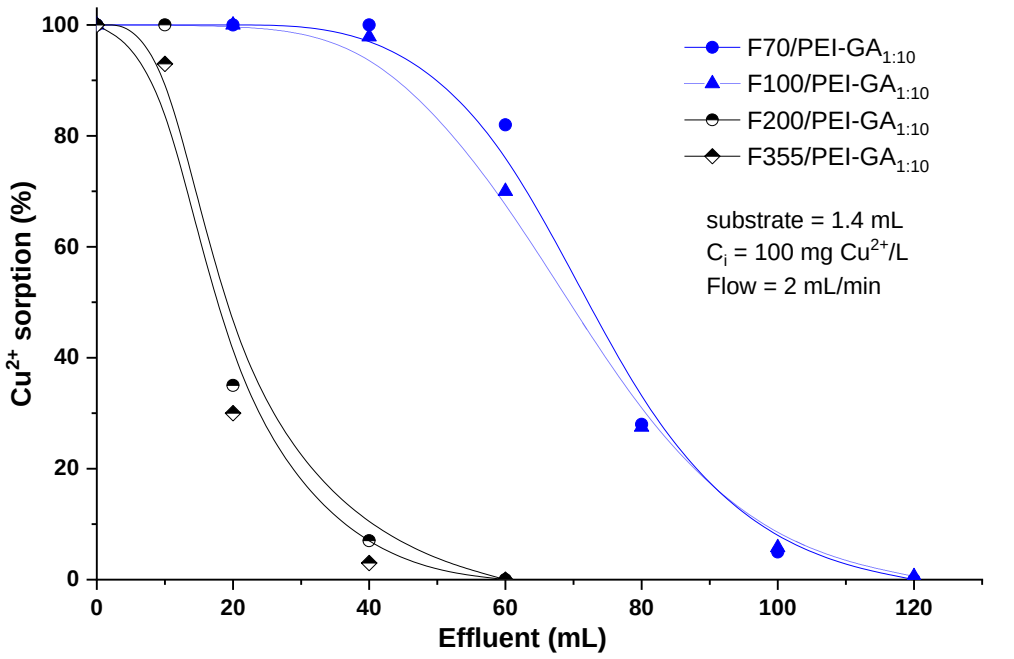

Figure 7. Sorbed amount (%) of Cu^{2+} onto different sand composites with low cross-linking degree using a dynamic experiment in a column.

The dynamic sorption experiments showed that the efficiency and maximum capacity of the composites depended on the thickness of the organic shell. The retention efficiency reached ~100% for the first 40 mL of influent solution in the case of the composites with the smallest cores (F70 and F100). The other composites recorded a drop-down of efficiency after 10 mL influent due to the smaller amount of organic shell on the sand grains. The breakthrough

time, t_b, increased in order F355/PEI-$GA_{1:10}$ (4 min) < F200/PEI-$GA_{1:10}$ (6 min) < F100/PEI-$GA_{1:10}$ (23 min) < F70/PEI-$GA_{1:10}$ (25 min) and depended on the quantity of PEI deposited on the core/shell sand composites. When C_e reached 95% of the influent concentration the exhaustion time, t_e, was reached which increased in the same order: F355/PEI-$GA_{1:10}$ (19 min) < F200/PEI-$GA_{1:10}$ (21 min) < F100/PEI-$GA_{1:10}$ (50 min) = F70/PEI-$GA_{1:10}$ (50 min). These results confirmed, once again, that the maximum sorption capacity depends on the organic shell on sand surface. Figure 8 shows the experimental breakthrough curves fitted by applying Thomas and Yoon–Nelson models [39] by linear regression.

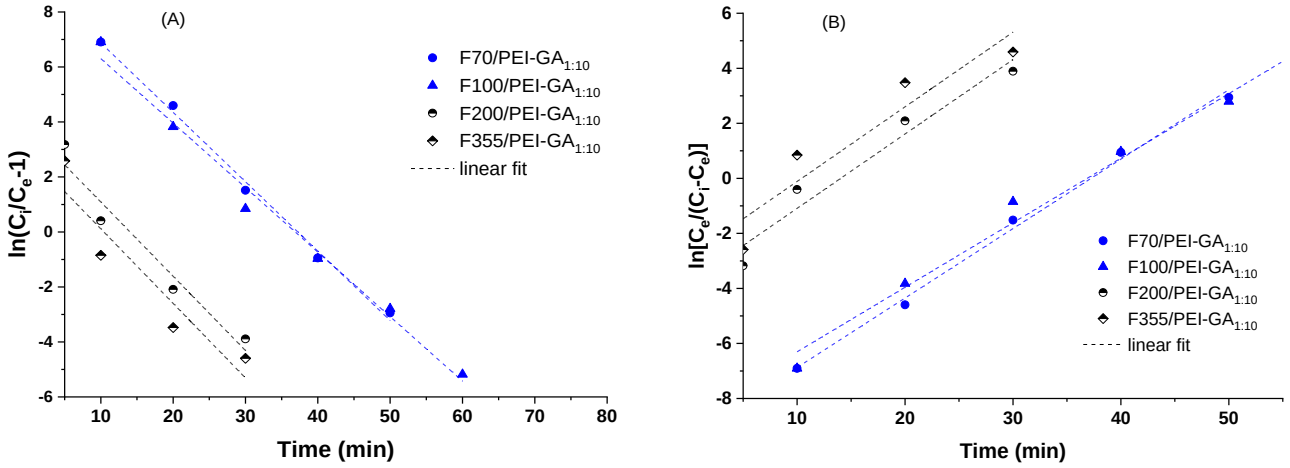

Figure 8. Linear plots of Thomas (**A**) and Yoon–Nelson (**B**) models for sand composites with different core sizes and the same cross-linking degree (x = 0.1).

The linear form of the Thomas model is expressed by Equation (2):

$$\ln(C_i/C_e - 1) = (k_{TH} \cdot q_{max} \cdot m)/Q - k_{TH} \cdot C_i \cdot t, \quad (2)$$

where C_i and C_e (mg/mL) are the influent and the effluent concentrations, respectively, k_{TH} is the Thomas model constant (mL/(mg·min)), q_{max} (mg/g) is the sorption capacity, m is the sorbent quantity, and Q (mL/min) is the flow rate.

The linear form of the Yoon–Nelson model is represented by Equation (3):

$$\ln[C_e/(C_i - C_e)] = k_{YN} \cdot t - \tau \cdot k_{YN}, \quad (3)$$

where k_{YN} (1/min) is the rate velocity constant and τ (min) is the time needed for 50% breakthrough of the sorbate.

The linear fit in Figure 8 enables the calculation of the parameters of both models, with Equations (2) and (3), resumed in Table 3. The R-square values, in the domain 0.8871–0.9954, showed a good fit of both models with the experimental data.

The value of the k_{YN} parameter is related to the diffusion, a characteristic of the mass transfer zone, MTZ, known as the efficiency of a sorbent as the size of the sorption zone in the chromatographic column. Thus, MTZ was calculated by the Equation (4):

$$MTZ = Z \cdot (1 - t_b/t_e), \quad (4)$$

where Z is the total depth of the sorbent in the column (40 mm).

Table 3. Parameters of dynamic sorption of Cu^{2+} onto sand composites determined by Thomas and Yoon–Nelson models.

Sorbent	Thomas Model			Yoon–Nelson Model		
	k_{TH} (mL/(min·mg))	q_{max} (mg/g)	R^2	k_{YN} (1/min)	T (min)	R^2
F70/PEI-$GA_{1:10}$	2.5	3.35	0.9954	0.25	38	0.9954
F100/PEI-$GA_{1:10}$	2.3	3.35	0.9880	0.23	38	0.9881
F200/PEI-$GA_{1:10}$	2.7	1.25	0.9499	0.27	14	0.9499
F355/PEI-$GA_{1:10}$	2.7	1.01	0.8871	0.27	11	0.8871

The differences of MTZ for the composites with small cores (20 mm for F70/PEI-$GA_{1:10}$ and 18.4 mm for F100/PEI-$GA_{1:10}$), and MTZ for the composites with big cores (11 and 8 mm for F200/PEI-$GA_{1:10}$ and F355/PEI-$GA_{1:10}$, respectively) demonstrated that the diffusion process of the Cu^{2+} ions was more pronounced for composites with a higher amount of organic shell. This fact was confirmed, also, by the Thomas constant which was smaller for the composites with smaller cores (Table 3). To further investigate the diffusion process which takes place inside the cross-linked shell of each composite, the efficiency and maximum capacity of sorption using the composites with the same core size (F100) but with the shell cross-linked at two ratios (r = 1:10, weak cross-linked and r = 1:1, strong cross-linked) were studied (Figure 9).

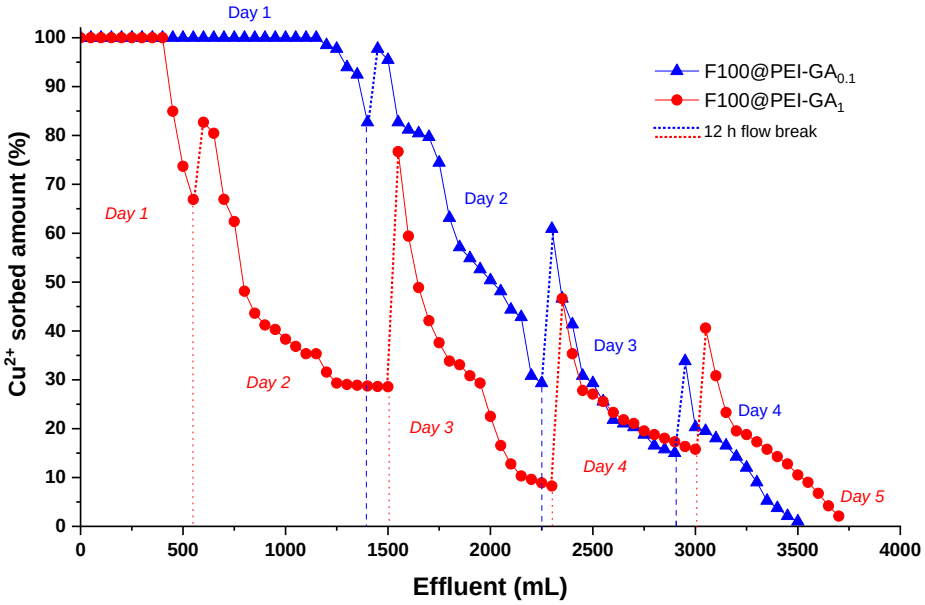

Figure 9. The amount of copper sorbed from an influent solution (C_{Cu2+} = 2 mg/L) onto F100/PEI-GA_r composites (r = 1:10 and 1:1) inside a column operated in a discontinuous mode (with 12 h break of flow before each run).

Using a dynamic set-up for the sorption of Cu^{2+} from a diluted solution (2 mg/L), with 12 h breaks (discontinuous mode), it was demonstrated that the composites with a higher cross-linking degree had a smaller efficiency (cleaning 400 mL solution) but a higher exhaustion time (after 3700 mL) as compared to the same composites with a lower degree of cross-linking, which clean 1200 mL water sample. This fact could be explained by the diffusion of Cu^{2+} ions through cross-linked polyelectrolyte chains when the hydrodynamic pressure was suppressed during the 12 h breaks. After each break, both composites presented higher sorption capacities compared with the previous day.

To evidence the possible application of the prepared sand composites for water purification, a column filled with F100/PEI-$GA_{1:5}$ was used for Cu^{2+} and BCG in a sorption/desorption cycle (Figure 10).

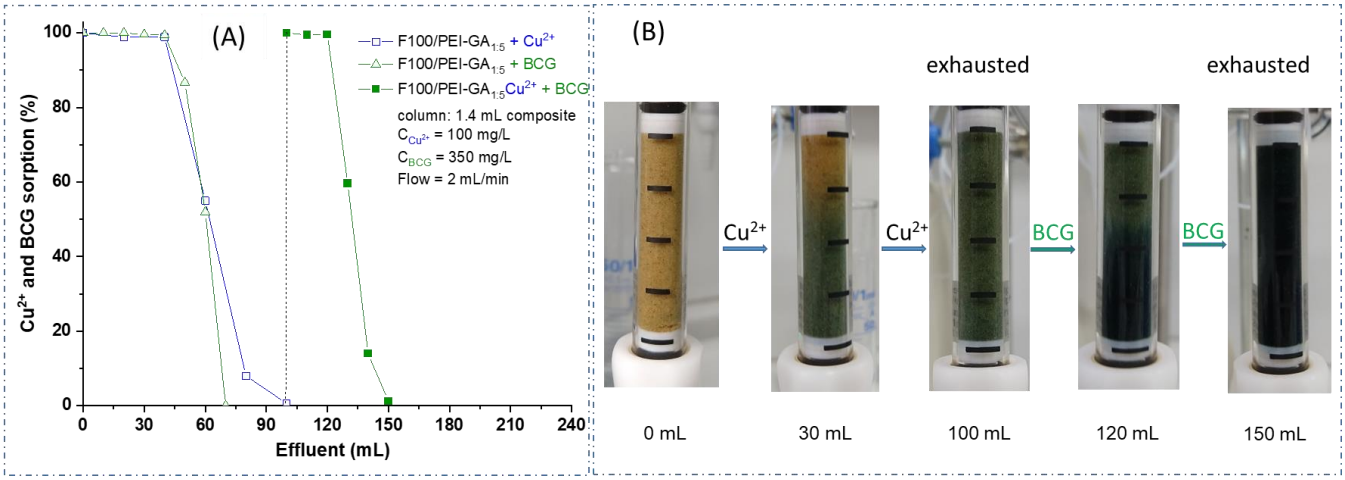

Figure 10. (**A**) Sorption efficiency of Cu^{2+} and BCG onto F100/PEI-$GA_{1:5}$ from mono-component influent solution carried out in separated runs (empty symbols) and consecutive runs (full symbols), where BCG has been retained by the material exhausted in Cu^{2+}; (**B**) Column images after different effluent volumes passed through.

In two independent experiments of dynamic sorption of Cu^{2+} and BCG onto F100/PEI-$GA_{1:5}$ it was shown that both types of model pollutants were almost 100% retained inside the column, the maximum sorbed amount being approximately 4 and 15 mg/mL column for Cu^{2+} and BCG, respectively. The Cu^{2+} interacted inside the cross-linked shell with the amino active groups of PEI by forming coordinative bonds, while the BCG dye molecule, with sulfonate groups, interacted electrostatically with the protonated amino groups of the composite surface. Moreover, the hydrogen bonds, π-stacking, and hydrophobic interactions could favor the retention as possible secondary forces. It was observed that the exhausted column filled with Cu^{2+} ions could further retain the BCG molecules (Figure 9, full squares), the sorbed amount, in this case, being 10 mg BCG/mL column, which represents approximately 75% of the amount of dye sorbed on the initial composite. The BCG molecules could be retained on the F100/PEI-$GA_{1:5}$ with copper inside through the Cu^{2+}/sulfonate attractive forces, where sulfonate could replace the anion sulfate in the coordination sphere of the immobilized Cu^{2+}. Moreover, BCG could also interact with the shell by the same balance of forces, (electrostatic, hydrogen bonds, π-stacking and hydrophobic interactions). The dynamic sorption of each pollutant in single or consecutive dynamic sorption, depicted in Figure 10B, enlightened two important aspects: (i) all pollutant species were completely sorbed by the composite when the competitive conditions were not reached, namely up to 40 mL effluent, and (ii) there was no competition between Cu^{2+} and BCG for the composite active sites, Cu^{2+} being bound through coordinative interactions while BCG was electrostatically bound.

To further investigate the strength of these interactions, which can be established between the pollutants and the active sites of the composites, the desorption of Cu^{2+} with $EDTANa_2$, and of BCG with NaOH (1 M), was carried out (Figure 11).

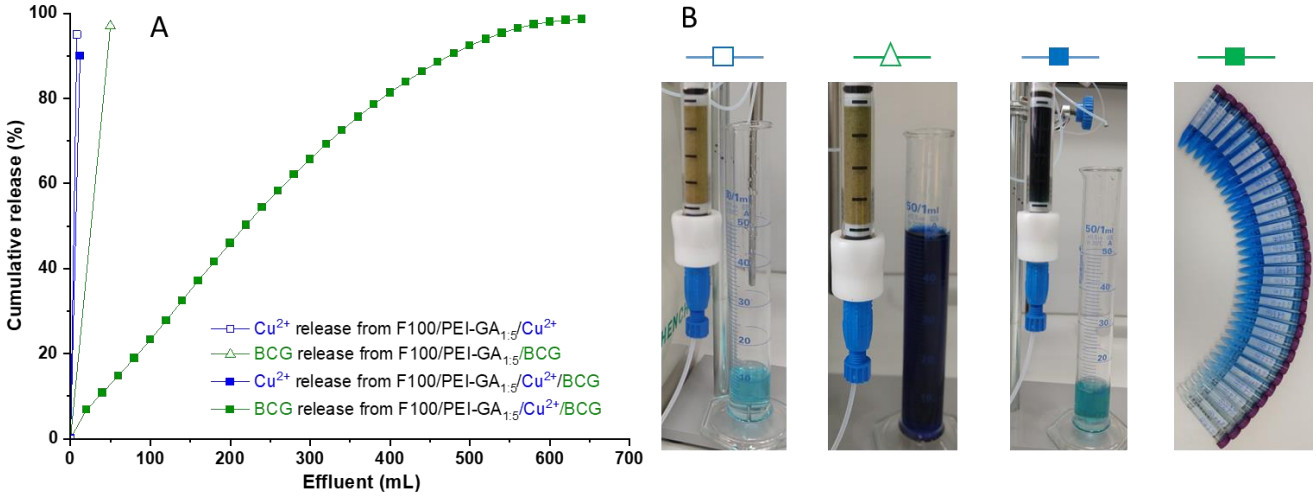

Figure 11. Desorption efficiency of Cu^{2+} and BCG from F100/PEI-$GA_{1:5}$ loaded with single components (empty symbols) and bi-components (full symbols) (**A**) evaluated in dynamic conditions (2 mL/min) in a column (**B**).

To determine the edge between coordinative and electrostatic interactions, the individual and consecutive desorption of Cu^{2+} and BCG were evaluated using the exhausted columns (F100/PEI-$GA_{1:5}$/Cu^{2+}, F100/PEI-$GA_{1:5}$/BCG and F100/PEI-$GA_{1:5}$/Cu^{2+}/BCG). The exhausted column loaded with Cu^{2+}, was washed with $EDTANa_2$ solution (0.01 M), removing thus the sorbed ions in the composite F100/PEI-$GA_{1:5}$/Cu^{2+} (Figure 11, empty squares) and to evaluate the desorbed amount (92% from the sorbed amount). The same desorption has been carried out starting with the column fully loaded with BCG, the desorbed amount (in basic medium) being more than 93% of the BCG sorbed amount. Thus, the desorption process of single components from exhausted columns had an efficiency higher than 90%. The column loaded with Cu^{2+} and BCG presented the same desorption pattern, but only if the Cu^{2+} was the first pollutant extracted from the exhausted column (F100/PEI-$GA_{1:5}$/Cu^{2+}/BCG). Instead, if the BCG was extracted in the presence of Cu^{2+} a ten time increase in the amount of NaOH effluent consumed to reach the same desorption efficiency was observed (Figure 10, full squares). This fact demonstrated strong interactions between BCG molecules and Cu^{2+} ions, besides the electrostatic forces established with PEI chains inside the cross-linked shell of the composites. This type of strong interaction of BCG-Cu^{2+} could be attributed to the previous replacement of sulfate ions in the coordination sphere of the PEI-Cu^{2+} complex. Respecting the order of effluents, $EDTANa_2$ followed by NaOH, both types of pollutants could be successfully removed from the column. A new sorption desorption cycle could be started after the regeneration of the F100/PEI-$GA_{1:5}$ with HCl and NaOH aqueous solution.

4. Conclusions

This study proposed to investigate: (1) the stability of sand core/shell composites obtained by the direct deposition of a nonstoichiometric polyelectrolyte complex, as a function of the core size and shell cross-linking degree and (2) the sorption/desorption in dynamic conditions of two model pollutants, Cu^{2+} and BCG. By swelling studies and XPS measurements, it was shown that the stability of the composites increased with the decrease in the sand grains size and with the cross-linking degree. The sorption tests on 12 prepared composite samples demonstrated that the sorbed amount of copper ions is influenced by the composite organic shell thickness. The consecutive sorption cycles of copper ions and BCG molecules, carried out in dynamic conditions, showed an additive capacity of the composites toward different types of pollutants, an important amount of BCG being sorbed in the exhausted column fully loaded with copper ions. The desorption process of both pollutants took place with very good yields and low consumption of

effluent solutions if the copper was desorbed first in $EDTANa_2$ solution. The consecutive sorption/desorption tests demonstrated the composite behavior depending on the types of interactions (coordinative vs. electrostatic) which can be established between pollutant molecules dissolved in aqueous media and the active sites of the composite surface. This study demonstrated that sand/polyelectrolyte composites are promising sorbents, are cheap and eco-friendly, and can find applications in water treatment by the loading/release of different types of pollutants. As further studies, the influence of the molar mass of polymers and the effluent flow speed will be followed to increase the polymer amount and the water cleaning yield, respectively.

Author Contributions: Investigation, methodology, data processing and analysis, writing original draft, project administration: F.B.; Methodology, investigation, data processing and analysis: M.-M.Z. and L.-M.P.; Data processing, formal analysis, and writing—review and editing: F.S. and M.M. All authors have read and agreed to the published version of the manuscript.

Funding: This work was supported by a grant of the Romanian Ministry of Research, Innovation and Digitization, CNCS/CCCDI-UEFISCDI, project number PN-III-P2-2.1-PED-2019-1996, within PNCDI III.

Acknowledgments: This work was supported by the research infrastructure developed through the European Social Fund for Regional Development, Competitiveness Operational Programme 2014–2020, Axis 1, Action: 1.1.3, Project "Infra SupraChem Lab-Center for Advanced Research in Supramolecular Chemistry" (Contract 339/390015/25.02.2021, cod MySMIS: 108983).

Conflicts of Interest: The authors declare that they have not competing financial interests or personal relationships that could influence this article.

References

1. Huang, D.-Y.; Wu, Y.; Jiang, Y.-J.; Zhang, M.-S.; Cheng, L.; He, S.-H.; Chen, B.-J. Rapid determination, pollution characteristics and risk evaluations of antibiotics in drinking water sources of Hainan, China. *Chin. J. Anal. Chem.* **2022**, *50*, 100164. [CrossRef]
2. Samsami, S.; Mohamadi, M.; Sarrafzadeh, M.-H.; Rene, E.R.; Firoozbahr, M. Recent advances in the treatment of dye-containing wastewater from textile industries: Overview and perspectives. *Process Saf. Environ. Prot.* **2020**, *143*, 138–163. [CrossRef]
3. Dragan, E.S.; Dinu, M.V. Advances in porous chitosan-based composite hydrogels: Synthesis and applications. *React. Funct. Polym.* **2020**, *146*, 104372. [CrossRef]
4. Ghiorghita, C.-A.; Mihai, M. Recent developments in layer-by-layer assembled systems application in water purification. *Chemosphere* **2021**, *270*, 129477. [CrossRef]
5. Lin, S.; Ali, M.U.; Zheng, C.; Cai, Z.; Wong, M.H. Toxic chemicals from uncontrolled e-waste recycling: Exposure, body burden health impact. *J. Hazard. Mater.* **2022**, *426*, 127792. [CrossRef]
6. Adeyemo, A.A.; Adeoye, I.O.; Bello, O.S. Adsorption of dyes using different types of clay: A review. *Appl. Water Sci.* **2017**, *7*, 543–568. [CrossRef]
7. Lapointe, M.; Barbeau, B. Understanting the roles and characterizing the intrinsic properties of synthetic vs. natural polymers to improve clarification through interparticle bridging: A review. *Sep. Purif. Technol.* **2020**, *231*, 115893. [CrossRef]
8. Mcyotto, F.; Wei, Q.; Macharia, D.K.; Huang, M.; Shen, C.; Chow, C.W.K. Effect of dye structure on color removal efficiency by coagulation. *Chem. Eng. J.* **2021**, *405*, 126674. [CrossRef]
9. Chakraborty, R.; Asthana, A.; Singh, A.K.; Jain, B.; Susan, A.B.H. Adsorption of heavy metal ions by various low-cost adsorbents: E review. *Int. J. Environ. Anal. Chem.* **2022**, *102*, 342–379. [CrossRef]
10. Mallakpour, S.; Hatami, M. An effective, low-cost and recyclable bio-adsorbent having amino acid intercalated LDH@Fe3O4/PVA magnetic nanocomposites for the removal of mehyl orange from aqueous solution. *Appl. Clay Sci.* **2019**, *174*, 127–137. [CrossRef]
11. Kumar, P.S.; Joshiba, G.J.; Femina, C.C.; Varshini, P.; Priyadharshini, S.; Karthick, M.S.A.; Jothirani, R. A critical review on recent developments in the low-cost adsorption of dyes from wastewater. *Desalin. Water Treat.* **2019**, *172*, 395–416. [CrossRef]
12. Weisspflog, J.; Gündel, A.; Vehlow, D.; Steinbach, C.; Müller, M.; Boldt, R.; Schwarz, S.; Schwarz, D. Solubility and selectivity effects of the anion on the adsorption of different heavy metal ions onto chitosan. *Molecules* **2020**, *25*, 2482. [CrossRef] [PubMed]
13. Saez, P.; Dinu, I.A.; Rodriguez, A.; Gomez, J.M.; Lazar, M.M.; Rossini, D.; Dinu, M.V. Composite cryo-beads of chitosan reinforced with natural zeolites with remarkable elasticity and switching on/off selectivity for heavy metal ions. *Int. J. Biol. Macromol.* **2020**, *164*, 2432–2449. [CrossRef] [PubMed]
14. Jaspal, D.; Malviya, A. Composites for wastewater purification: A review. *Chemosphere* **2020**, *246*, 125788. [CrossRef]
15. Ajith, M.P.; Aswathi, M.; Priyadarshini, E.; Rajamani, P. Recent innovations of nanotechnology in water treatment: A comprehensive review. *Bioresour. Technol.* **2021**, *342*, 126000. [CrossRef]

16. Islam, A.; Teo, S.H.; Taufiq-Yap, Y.H.; Ng, C.H.; Vo, D.-V.N.; Ibrahim, M.L.; Hasan, M.; Khan, M.A.R.; Nur, A.S.M.; Awual, R. Step towards the sustainable toxic dyes removal and recycling from aqueous solution—A comprehensive review. *Resour. Conserv. Recycl.* **2021**, *175*, 105849. [CrossRef]
17. Zhou, X.; Liang, J.-T.; Andersen, C.D.; Cai, J.; Lin, Y.-Y. Enhanced adsorption of anionic surfactants on negatively charged quartz sand grains treated with cationic polyelectrolyte complex nanoparticles. *Colloids Surf. A* **2018**, *553*, 397–405. [CrossRef]
18. Sangeetha, K.; Vidhya, G.; Vasugi, G.; Girija, E.K. Lead and cadmium removal from single and binary metal ion solution by novel hydroxyapatite/alginate/gelatin nanocomposites. *J. Environ. Chem. Eng.* **2018**, *6*, 1118–1126. [CrossRef]
19. Zdarta, J.; Degorska, O.; Jankowska, K.; Rybarczyk, A.; Piasek, A.; Ciesielczyk, F.; Jesionowski, T. Removal of persistent sulfamethoxazole and carbamazepine from water by horseradish peroxidase encapsulated into poly(vinyl chloride) electrospun fibers. *Int. J. Mol. Sci.* **2022**, *23*, 272. [CrossRef]
20. Zaharia, M.; Bucatariu, F.; Vasiliu, A.-L.; Mihai, M. Stable and reusable acrylic ion-exchangers. From HMIs highly polluted tailing pond to safe and clean water. *Chemosphere* **2022**, *304*, 135383. [CrossRef]
21. Morosanu, I.; Paduraru, C.; Bucatariu, F.; Fighir, D.; Mihai, M.; Teodosiu, C. Shaping polyelectrolyte composites for heavy metals adsorption from wastewater: Experimental assessment and equilibrium studies. *J. Environ. Manag.* **2022**, *321*, 115999. [CrossRef] [PubMed]
22. Wang, J.; Yang, Q.; Zhang, L.; Liu, M.; Hu, N.; Zhang, W.; Zhu, W.; Wang, R.; Suo, Y.; Wang, J. A hybrid monolithic column based on layered double hydroxide-alginate hydrogel for selective solid phase extraction of lead ions in food and water samples. *Food Chem.* **2018**, *257*, 155–162. [CrossRef] [PubMed]
23. Demarchi, C.A.; Campos, M.; Rodrigues, C.A. Adsorption of textile dye Reactive Red 120 by chitosan-Fe(III)-crosslinked: Batch and fixed-bed studies. *J. Environ. Chem. Eng.* **2013**, *1*, 1350–1358. [CrossRef]
24. Dinu, M.V.; Humelnicu, D.; Lazar, M.M. Analysis of copper(II), cobalt(II) and iron(III) sorption in binary and ternary systems by chitosan-based composite sponges obtained by ice-segregation approach. *Gels* **2021**, *7*, 103. [CrossRef]
25. Nicola, R.; Costisor, O.; Muntean, S.-G.; Nistor, M.-A.; Putz, A.-M.; Ianasi, C.; Lazau, R.; Almasy, L.; Sacarescu, L. Mesoporous magnetic nanocomposites: A promising adsorbent for the removal of dyes from aqueous solutions. *J. Porous Mater.* **2020**, *27*, 413–428. [CrossRef]
26. Deng, J.; Liu, Y.; Liu, S.; Zeng, G.; Tan, X.; Huang, B.; Tang, X.; Wang, S.; Hua, Q.; Yan, Z. Competitive adsorption of Pb(II), Cd(II) and Cu(II) onto chitosan-pyromellitic dianhydride modified biochar. *J. Colloid Interface Sci.* **2017**, *506*, 355–364. [CrossRef]
27. Feng, Y.; Wang, Y.; Wang, Y.; Zhang, X.-F.; Yao, J. In-situ gelation of sodium alginate supported on melamine sponge for efficient removal of copper ions. *J. Colloid Interface Sci.* **2018**, *512*, 7–13. [CrossRef]
28. Saravanan, A.; Thamarai, P.; Kumar, P.S.; Rangasamy, G. Recent advances in polymer composite, extraction, and their application for wastewater treatment: A review. *Chemosphere* **2022**, *308*, 136368. [CrossRef]
29. Guo, D.-M.; An, Q.-D.; Li, R.; Xiao, Z.-Y.; Zhai, S.-R. Ultrahigh selective and efficient removal of anionic dyes by recyclable polythyleneimine-modified cellulose aerogels in batch and fixed-bed systems. *Colloids Surf. A* **2018**, *555*, 150–160. [CrossRef]
30. Lopez-Cervantes, J.; Sanchez-Machado, D.-I.; Sanchez-Duarte, R.G.; Correa-Murrieta, M.A. Study of a fixed-bed column in the adsorption of an azo dye from an aqueous medium using a chitosan-glutaraldehyde biosorbent. *Adsorpt. Sci. Technol.* **2018**, *36*, 215–232. [CrossRef]
31. Abtahi, S.M.; Marbelia, L.; Gebreyohannes, A.Y.; Ahmadiannamini, P.; Joannis-Cassan, C.; Albasi, C.; de Vos, W.M.; Vankelecom, I.V.J. Micropollutant rejection of annealed polyelectrolyte multilayer based nanofiltration membranes for treatment of conventionally-treated municipal wastewater. *Sep. Purif. Technol.* **2019**, *209*, 470–481. [CrossRef]
32. Bucatariu, F.; Ghiorghita, C.-A.; Zaharia, M.; Schwarz, S.; Simon, F.; Mihai, M. Removal and separation of heavy metal ions from multicomponent simulated waters using silica/polyethyleneimine composite microparticles. *ACS Appl. Mater. Interfaces* **2020**, *12*, 37585–37596. [CrossRef] [PubMed]
33. Bucatariu, F.; Schwarz, D.; Zaharia, M.; Steinbach, C.; Ghiorghita, C.-A.; Schwarz, S.; Mihai, M. Nanostructured polymer composites for selective heavy metal ion sorption. *Colloids Surf. A* **2020**, *603*, 125211. [CrossRef]
34. Bucatariu, F.; Petrila, L.-M.; Teodosiu, C.; Mihai, M. Versatile nanostructured SiO2/cross-linked polyelectrolyte composites for emrging pollutants removal from aqueous media. *C. R. Chim.* **2022**, *25*, 95–108.
35. Bucatariu, F.; Zaharia, M.-M.; Petrila, L.-M.; Simon, F.; Mihai, M. Sand/polyethyleneimine composite microparticles: Eco-friendly, high selective and efficient heavy metal ion catchers. *Colloids Surf. A Physicochem. Eng. Asp.* **2022**, *649*, 129540. [CrossRef]
36. Shao, H.; Ding, Y.; Hong, X.; Liu, Y. Ultra-facile and rapid colorimetric detection of Cu^{2+} with branched polyethylenimine in 100% aqueous solution. *Analyst* **2018**, *143*, 409–414. [CrossRef] [PubMed]
37. Ouachtak, H.; Akhouairi, S.; Haounati, R.; Addi, A.A.; Jada, A.; Tahaa, M.L.; Douch, J. 3,4-Dihydroxybenzoic acid removal from water by goethite modified natural sand column fixed-bed: Experimental study and mathematical modeling. *Desalin. Water Treat.* **2020**, *194*, 439–449. [CrossRef]
38. He, M.; Yan, W.; Chang, Y.; Liu, K.; Liu, X. Fundamental infrared absorption features of α-quartz: An unpolarized single-crystal absorption infrared spectroscopic study. *Vib. Spectrosc.* **2019**, *101*, 52–63. [CrossRef]
39. Yoon, Y.H.; Nelson, J.H. Breakthrough Time and Adsorption Capacity of Respirator Cartridges. *Am. Ind. Hyg. Assoc. J.* **1992**, *53*, 303–316. [CrossRef]